On the Metal Cutting Mechanism with the Built-up Edge

Koichi HOSHI*
Tetsutaro HOSHI**
(Received August 31, 1968)

Abstracts

An experimental study was undertaken in order to study the formation and the cutting mechanism of the built-up edge.

Investigations of the quick-stopped partly formed chip produced at various cutting parameters clearly demonstrated that the secondary plastic flow in chip formation was the direct source of the work-hardened metal which forms the built-up layer or the built-up edge. Adhesion of the built-up edge nucleus onto the tool face was discussed from the mechanical inlaying principle.

Growth and fracture of the typical built-up edge and the metal cutting model were described. Variation of the built-up edge and the metal cutting model geometries were explored by a series of quick-stop tests, and the test results were processed by a computer simulation of the cutting force equilibrium, which results indicated that the variation of the cutting force was mainly controlled by the contact length between the built-up edge and the chip.

Contents

* Precision Engineering Laboratory, Faculty of Engineering, Hokkaido University, Sapporo, Japan.
** Precision Engineering Laboratory, Faculty of Engineering, Kyoto University, Kyoto, Japan.

1. Introduction.

In the history of metal cutting research, the built-up edge has been one of the most interesting subjects[1)-6)], and is still producing diversified discussions. One of the authors has continued to work on[7),8)] this problematic point; recently, he finished a series of metal cutting tests from which many formerly uncovered facts came to light.

In this study, orthogonal cutting of carbon steels were investigated for the purpose of obtaining advanced knowledges on the formation of the built-up edge and the metal cutting mechanism when it was present.

In particular, the following points were explored:—

1) the type of the physical process by which a portion of the work metal was deformed to form the built-up edge;
2) the type of adhesion of the built-up edge material onto the tool face;
3) the metal removal model by which the worked metal plastically transformed into chips when the built-up edge was present;
4) the manner in which the size and shape of the built-up edge varied according to the change in cutting speed and tool rake angle; also periodical fluctuations of the built-up edge in a cutting at a given condition were observed; and the cause of such variations were studied.

Experimental data were presented in the form of micro-photographs of the middle sections of the partly formed chips obtained by quick-stopping the orthogonal turning tests of the steel tube ends, at cutting speeds ranging from 8 mpm (meters per minute) to 165 mpm. By those micro-photographs, the size and shape of the built-up edge were analyzed, its formation and cutting mechanism were estimated, and a simplified metal flow model was proposed, which was further followed by a simulation of mechanical force equilibrium in cutting with the built-up edge.

2. Material and equipment for the study.

For the quick-stop tests to obtain the partly formed orthogonal chip having a built-up edge, a tubular work piece was machined beforehand out of a solid block of 0.25% carbon steel with mechanical properties and compositions as listed below.

Mechanical properties of material.

Yielding point kg/mm²	Tensile strength kg/mm²	Total elongation %	Reduction of area %	Hardness H_B	Impact value kg-m/cm²
30.7	52.6	34.7	58.0	145	5.1

Chemical composition of material (wt. %)

C	Si	Mn	P	S	Ni	Cr	Mo	Cu
0.24	0.30	0.68	0.015	0.012	0.14	0.13	0.04	0.28

The quick-stop orthogonal turning tests employed P20 carbide tools and also 5% Co and 10% Co type high speed steel tools. The tool was mounted on a quick-stop device fixed in such a way that the tool could be suddenly removed along the direction of cutting, from the cutting position.

The speed of the tool escape was preliminarily calibrated using high speed flash light photography as shown in Fig. 1. From the 170 mpm initial average

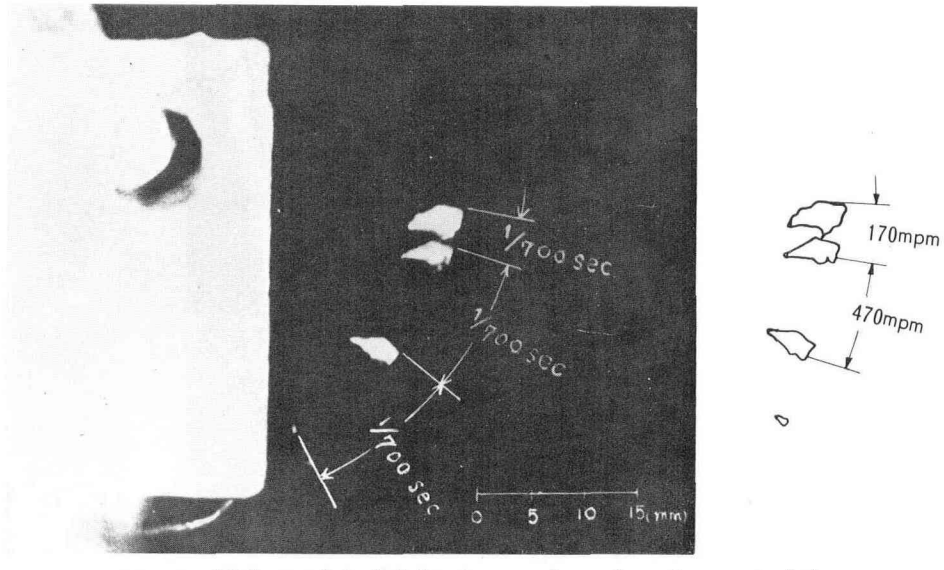

Fig. 1. High speed flash light photograph to show the speed of the escaping tool when the cutting process is quick-stopped. The average speed of the escaping tool is found to be 170 mpm during the initial 1/700 sec, followed by a constant speed of 470 mpm.

speed calculated from the photograph, the test rig was found to be capable of stopping the cutting without interfering with the chip formation from a cutting speed of 65 mpm or below.

The quick-stop tests were performed on an engine lathe Shoun-Cazeneuve, having a 500 mm swing over bed, a 1,000 mm distance between centers and a variable speed spindle drive motor rated at 11 kw.

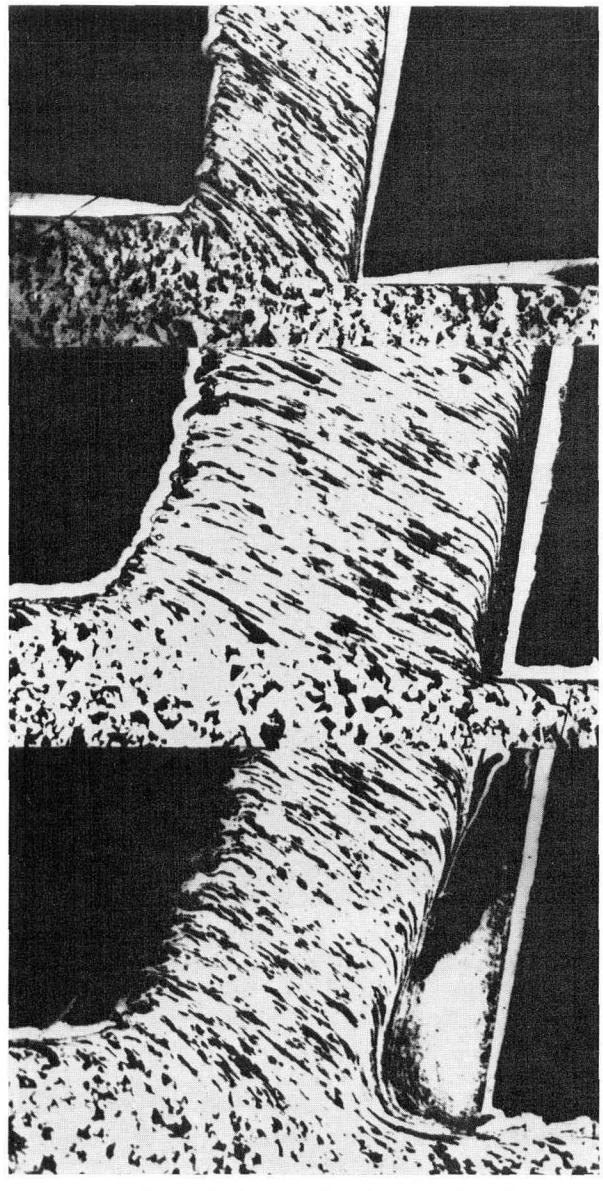

Fig. 2. Typical photographs showing the effect of cutting speed on the built-up edge.

3. Experimental results and interpretations.

3.1. Formation of built-up edge.

3.1.1. Secondary flow, built-up layer and built-up edge.

Partly formed chip quick-stopped from various cutting speeds contain built-up edges of different size. In a series of micro-photographs shown in Fig. 2, the specimen of a relatively high cutting speed, top picture (a) at 188 mpm, involves no built-up edge, but only a flow of metal along the tool face which is conventionally termed as "the secondary flow". A 20 to 30 μ ($\mu = 10^{-3}$ mm) thick secondary flow zone is observed at the cutting speed of 130 mpm and above.

At slower cutting, a layer of stationary metal is observed between the secondary flow and the tool face as shown in the figure taken at 41 mpm, Fig. 2 (b). Micro-hardness tests indicated that this kind of layer (297 to 322 Hv) was as hard as the typically formed built-up edge (297 to 439 Hv) and was more work-hardened than the original work piece (153 to 159 Hv) or the formed chip (236 to 256 Hv). The stationary layer is the bulk of metal formed by the secondary flow, thus it becomes work-hardened and stationary. The removed chip is separated from this layer by the secondary flow inside the chip. The

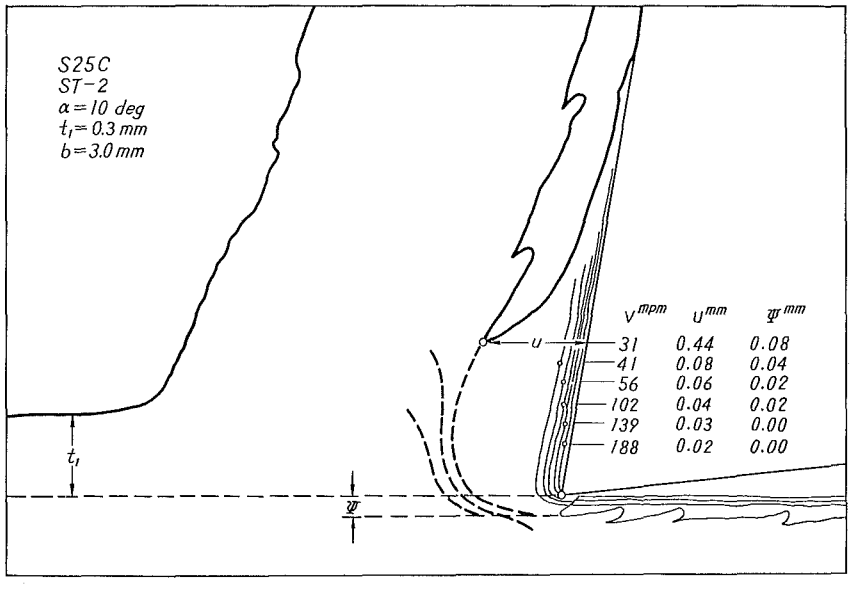

Fig. 3. Effect of cutting speed on the thickness u and the over-cut depth ψ of the built-up edge, depicted from the quick-stopped photographs.

thickness of the layer increases when the cutting speed is reduced, as shown in Fig. 3, until the layer attains the size of a typical built-up edge such as that seen at 35 mpm as shown in Fig. 2 (c). Therefore, it is proposed that this layer be tentatively referred to as the "built-up layer" and may by treated as a premature body of the built-up edge according to the definition as listed below.

Proposed definition of built-up layer and built-up edge

	Thickness u as indicated in Fig. 3 [mm]	Typical cutting speed range in steel cutting [mpm]
built-up layer	0 to 0.1	40 to 130
built-up edge	0.1 and above	under 40

Above the speed range of the built-up layer, only the secondary flow zone exists.

In a magnified view of the typically formed built-up edge (Fig. 4), there appears no clear boundary between the built-up edge and the removed chip. The flow of structure indicates that a secondary flow is occurring between the stationary metal and the removed chip. Since the metal is work-hardened by the secondary flow, a portion of metal joins up with the built-up edge as a new addition to it. Thus, the built-up edge constantly tends to grow in size as long as the metal in the secondary flow zone is work-hardenable. At a higher cutting speed, however, the metal is less work-hardenable due to the higher cutting temperature; therefore, the secondary flow zone loses its hardenability as soon as a thinner built-up layer is formed. Hence, the layer does not grow further.

3. 1. 2. Growth and fracture of built-up edge.

When a cutting is started, a layer of initially cut metal is work-hardened due to the secondary flow and adhered to the tool face to form a nucleus of the built-up edge. As seen in the example of Fig. 5, a continuous secondary flow occurs outside the nuclear layer, so much so that the metal is continuously work-hardened and added to the nuclear layer; as a result, a built-up edge is brought up to its typical size as shown by the dotted curve DEG in Fig. 6, in an extremely short time after the starting of cutting.

In its formation process, the built-up edge grows not only in the cutting direction but also toward the generated surface. The growth in the latter direction results in metal removal in excess of the given depth of cut. The over-cut depth is empirically proportional to the thickness u of the built-up edge, so that the following approximation holds

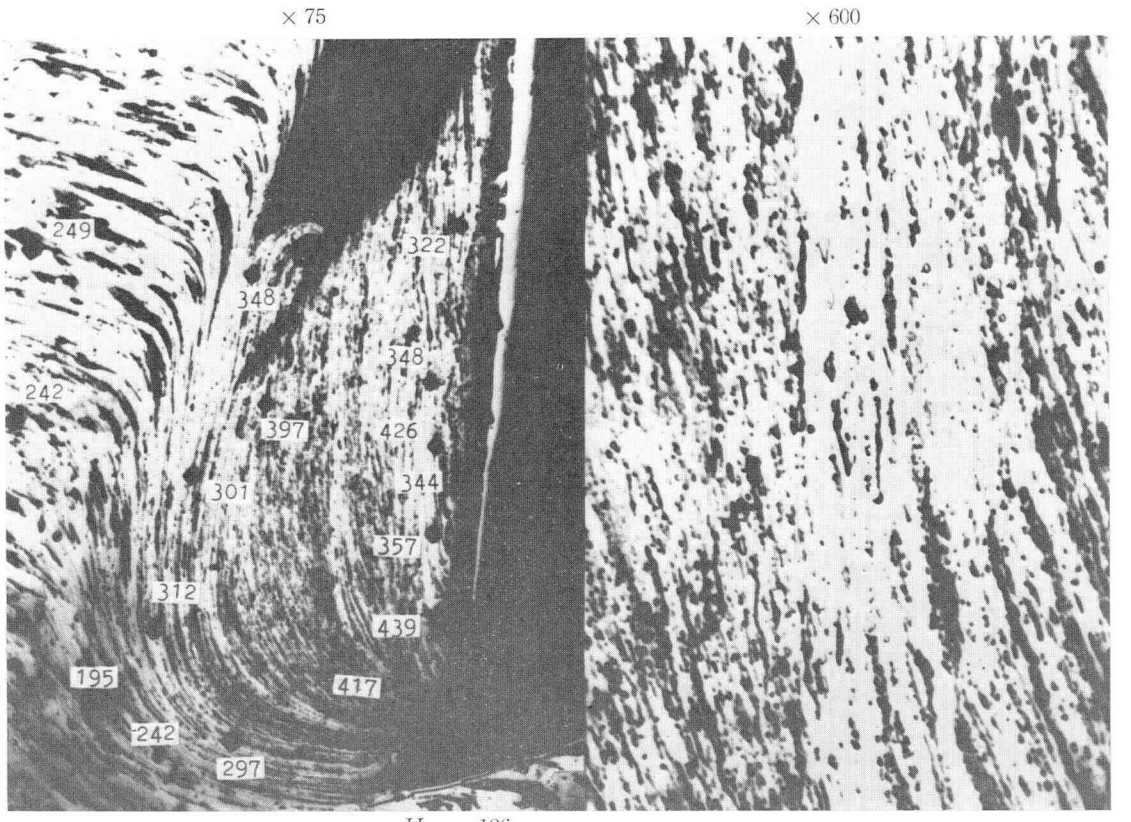

Fig. 4. Magnified view of the built-up edge found on a 10 deg rake angle carbide P20 tool at a cutting of 10 mpm speed and 0.3 mm depth. Numbers in the left photograph indicate the reading of Micro-Vickers hardness test at room temperature.

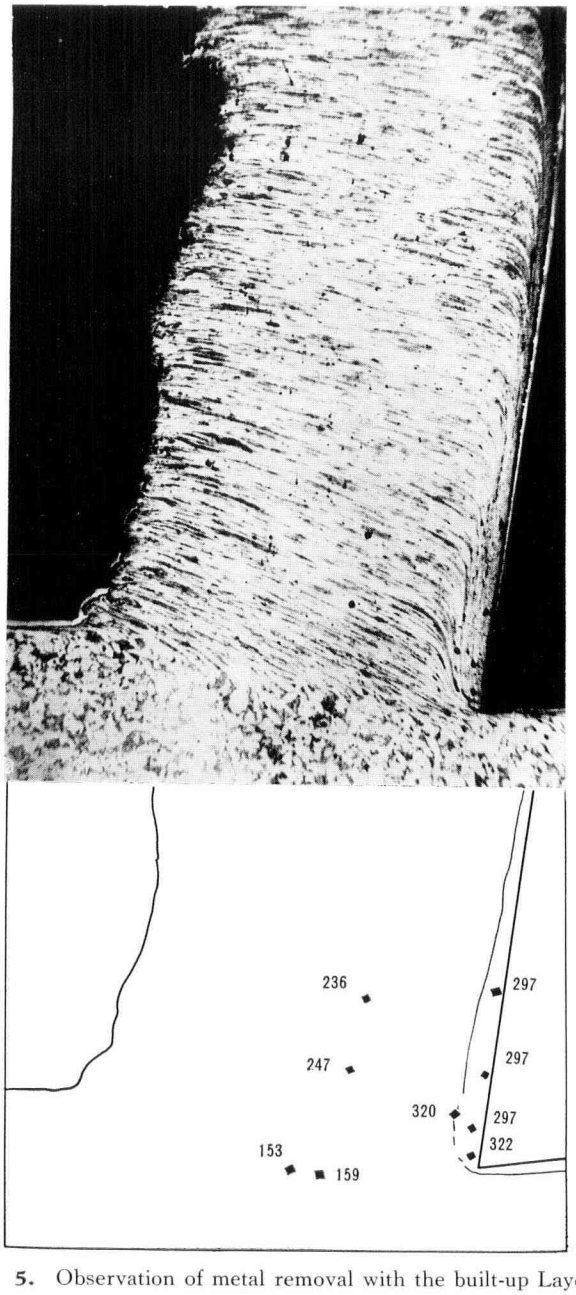

Fig. 5. Observation of metal removal with the built-up Layer.

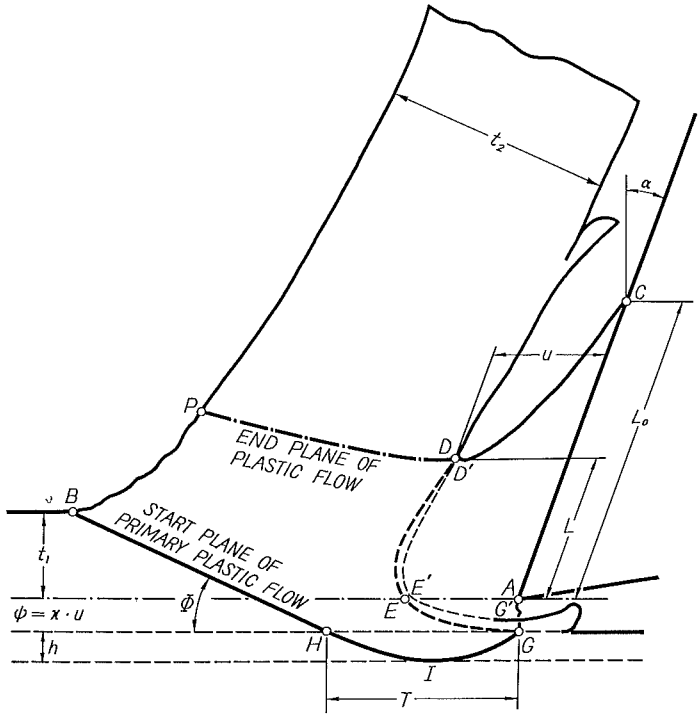

Fig. 6. Proposed model of metal cutting with the built-up edge.

$$\psi = k \cdot u$$

where k is a constant with a value lying around 0.283.

At a low cutting speed, the metal in the secondary flow zone is always work-hardenable even after the built-up edge attains its typical size. Thus the built-up edge continually grows in width and depth.

When it grows, however, to such a size that the shearing stress along an inner boundary such as D'E'G' (Fig. 6) exceeds a certain limit, fracture occurs along the inner boundary and the upper part of the fractured layer DEE'D' slides up with the chip while the lower part EGG'E' slides down to remain over the generated surface. The built-up edge continues another growth after the fracture so that the growth and fracture alternates periodically, maintaining an average size of the built-up edge representative of the given set of catting conditions.

3. 1. 3. Adhesion of built-up edge nucleus.

Past knowledge explains that the built-up edge adheres to the tool face

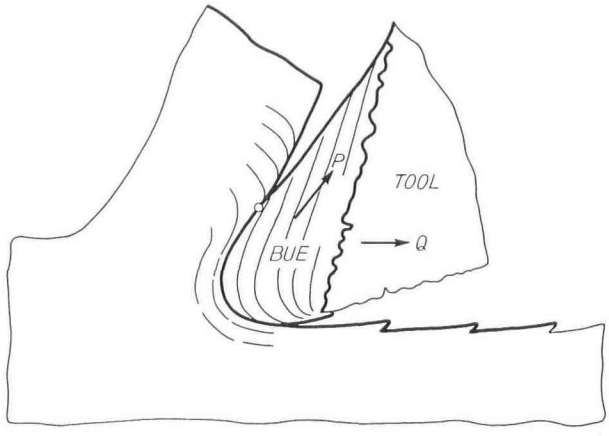

Fig. 7. Inlaying of the built-up edge onto the tool surface.

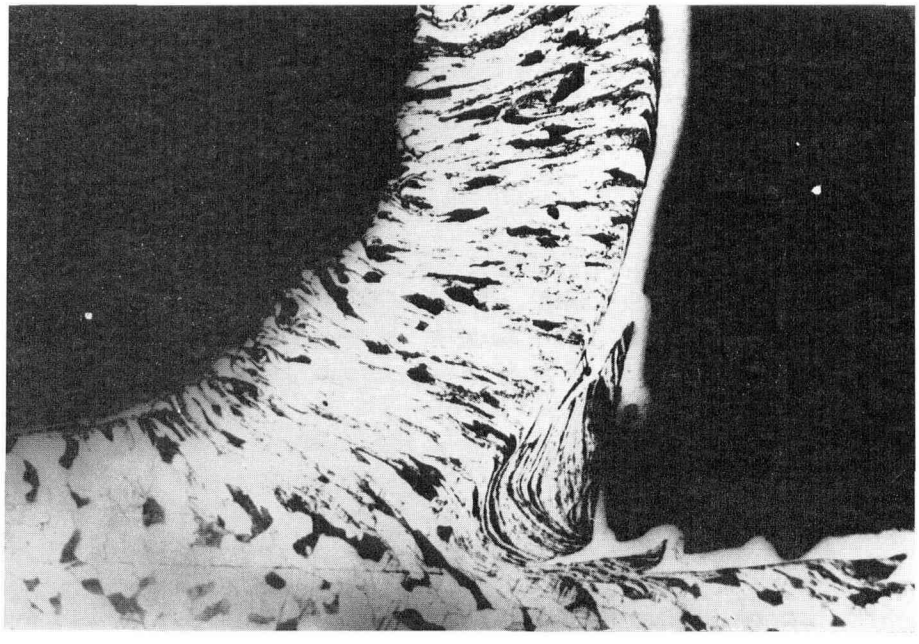

Fig. 8. Example of the buil-up edge formed at an extremely low cutting speed. 0.15C steel was being cut at 28 mm per min. speed and 0.1 mm depth by a 8 deg rake angle high speed steel tool (10% Co type).

by a kind of welding process resulting from the high stress and temperature of cutting. In addition to the theory above described, the present study suggests that the mechanical inlaying of the deformed metal into the asperities of the tool surface as depicted in Fig. 7, is one of the primary causes of the adhesion based on the following observations.

First, the built-up edge occurs at an extremely slow cut of small depth. Fig. 8 shows a built-up edge formed in a 0.1 mm deep cut at 28 mm per minute speed. Cutting temperature measured even at a higher cutting speed (1081 mm per min., work metal; brass) indicated that the maximum temperature was only 105 deg C registered near the tool-chip interface as seen in Fig. 9. According

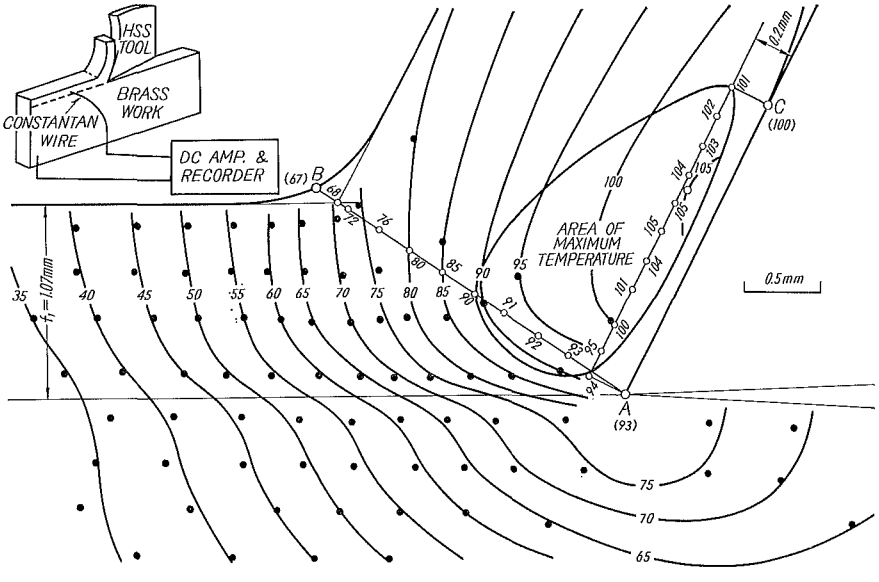

Fig. 9. Cutting temperature measured by the embedded constantan wire at a low speed cutting. Numbers indicate temperatures in deg C. Work material: 60% Cu brass, Pb under 0.3%, T.S. above 36 kg/mm², Tool material: 10% Co type HSS, room temperature: 18.3 deg C, tool rake angle $\alpha=25$ deg, cutting speed $v=1081$ mm per min, depth of cut $t=1.07$ mm. 0.17 mm dia. constantan wire put in 0.2 mm dia. hole.

to the conventional welding theory, adhesion is not likely to occur at such a low cutting temperature.

Second, all of the quick-stopped partly formed chips are left with the built-up edge, while the built-up edge is always left on the tool face when the cutting is finished in the conventional manner instead of quick-stopping. This indicates that the built-up edge is anchored to the tool face strongly against

the force acting parallel to the tool face as force P in Fig. 7, but weakly against the horizontal force Q which exerts itself at the instant of quick-stopping.

3. 2. Metal cutting model with built-up edge.

Although the hardness of the built-up edge is measured at room temperature at about three times higher than that of the original work metal, this must not lead to an interpretation that the built-up edge is acting as a substitute of the cutting tool on which the chip slides. Instead, the chip and the built-up edge are actually a continuous body and are separated by the shear of the secondary plastic flow.

A model as depicted in the Fig. 6 is proposed to explain the chip formation with the built-up edge. Tool-chip contact length is L_0 at the start of a cutting; though, as the built-up edge grows, the contact length is reduced to L and the over-cut of a depth ϕ occurs. The boundary where the original work metal firstly undergoes plastic flow is indicated by the curve BHIG. The plastic flow in the region of BHIG produces a deformed layer of a depth h left over from the generated surface. The largest portion of the primary plastic flow occurs right after the metal passes the boundary curve BHIG, and the rest of the plastic flow continues slowly until the metal reaches an end boundary curve somewhat like the curve PD. Although no clear-cut boundary of built-up edge exists, it may be well surmized that the stationary pile of work-hardened metal lies between the dotted curve passing through point E and the tool face, where point E is the intersection of the line of cutting direction passing through the tool tip point A and a line parallel to the tool face passing through point D where the chip escapes from contact with the built-up edge.

It is commonly known that the presence of a built-up edge at the tool tip reduces the cutting force. The reason for this was formerly sought based on the assumption that the face slope of the built-up edge served as a tool face with an increased rake angle so that the chip was formed in a shear plane with an increased shear angle. However, the chip formations observed in the present study did not agree with the above theory. First of all, the chip departs from the built-up edge at point D (Fig. 6) and does not slide over the face slope DC. Real contact length L between the chip and the built-up edge is at only a small portion of the surface of the built-up edge. Second, the built-up edge does not have a sharp edge but has a round tip so that it is impossible to define a simple shear plane in which most of the chip formation takes place.

When the metal cutting involves the built-up edge, the chip formation should be discussed on a more complex model than the conventional shear

plane concept. The following chapter will present results of an experimental study on the geometries of the metal cutting model as proposed in the Fig. 6 under variations in cutting parameters.

3. 3. Metal cutting model geometries under various cutting parameters.

3. 3. 1. Test procedure.

A total of 44 quick-stop cutting tests were carefully planned to investigate the effect of the size fluctuation of the built-up edge, the cutting speed, and the tool rake angle on the geometries of the metal cutting model. On every

TABLE 1. Test records of cutting geometries by change in cutting speed v.

S25C, SKH3, $\alpha=19.2$ deg, $t_1=0.3$ mm

Test No.	mpm v	mm u	mm L	mm ψ	mm t_2	mm h	deg Φ	mm T	mm L	ψ/u k	L/u m
1	8	0.64	(0.80)	0.20	0.82	0.20	25	0.90	1.46	0.30	(1.2)
4	10	0.52	0.35	0.18	0.76	0.11	25	0.55	0.84	0.34	0.69
2	10	0.36	0.36	0.12	0.70	0.10	27	0.60	0.81	0.33	1.0
3	10	0.27	0.44	0.10	0.70	0.08	26	0.53	0.85	0.37	1.6
16	17	0.45	0.56	0.10	0.75	0.09	25	0.68	1.22	0.20	1.2
10	17	0.42	0.37	0.08	0.62	0.08	26	0.60	1.10	0.19	0.9
7	17	0.40	0.43	0.14	0.78	0.09	27	0.70	1.60	0.33	1.1
5	17	0.40	0.50	0.11	0.90	0.10	25	0.72	1.00	0.28	1.2
6	17	0.39	0.43	0.11	0.60	0.10	29	0.53	0.90	0.30	1.1
11	17	0.35	0.30	0.09	0.70	0.08	27	0.57	0.53	0.26	0.85
13	17	0.30	0.30	0.09	0.68	0.08	26	0.48	1.10	0.30	1.0
8	17	0.30	(0.60)	0.08	0.70	0.08	25	0.55	1.60	0.27	*
9	17	0.30	0.33	0.08	0.63	0.08	25	0.49	0.55	0.27	1.1
12	17	0.28	0.37	0.09	0.62	0.07	26	0.37	0.70	0.32	1.3
14	17	0.20	0.26	0.09	0.69	0.06	27	0.44	0.64	0.45	1.3
15	17	0.20	0.37	0.08	0.60	0.06	25	0.38	0.60	0.40	1.8
17	31	0.42	0.80	0.08	0.77	0.08	27	0.80	1.86	0.20	1.9
18	31	0.28	0.75	0.05	0.66	0.06	27	0.40	1.70	0.13	1.9
20	41	0.24	(0.80)	0.03	0.80	0.05	26	0.73		0.12	3.3
19	41	0.16	(0.65)	0.03	0.80	0.05	27	0.48		0.20	4.0
21	56	0.05	(1.10)	0.01	0.90	0.04	25	0.52		0.20	(22)
22	70	0.06	(0.73)	0.01	0.80	0.04	27	0.40		0.13	12
23	165	0		0	0.65	0.04	25	0.15	0.94		

micro-photograph of the partly formed chip, characteristic geometries such as the thickness of the built-up edge u, contact length L etc. were readily obtained as listed in Table 1 and Table 2 from the pattern of the metal flow. Statical tests were applied on those data to identify the response of those geometries to the investigated effects, and the conclusions were drawn as summarized in Table 3.

TABLE 2. Test records of cutting geometries by change in tool rake angle α.

S25C, SKH3, $v=17$ mpm

Test No.	deg α	mm t_1	mm t_2	mm u	mm L	mm ϕ	mm h	mm T	deg Φ	ϕ/u k	L/u m
24	−11.0	0.30	0.87	0.95	0.76	0.30	0.24	1.51	25	0.31	0.80
25	− 5.8	0.30	0.87	0.73	0.62	0.27	0.23	0.98	24	0.37	0.85
26	− 5.8	0.23	0.88	0.77	0.98	0.23	0.20	1.41	25	0.30	1.20
27	0	0.33	0.66	0.55	0.66	0.16	0.16	0.71	27	0.29	1.20
28	0	0.10	*	0.73	0.23	0.27	0.23	1.02	38	0.37	0.32
29	4.2	0.20	0.95	0.44	0.51	0.13	0.16	1.22	22	0.30	1.20
30	4.2	0.30	1.04	0.42	0.53	0.16	0.16	0.84	23	0.38	1.20
31	9.0	0.30	1.04	0.44	0.66	0.16	0.16	1.00	22	0.36	1.50
32	9.0	0.30	0.66	0.38	0.55	0.13	0.13	0.70	27	0.34	1.50
33	9.0	0.27	0.75	0.27	0.51	0.13	0.15	0.43	26	0.48	1 90
34	14.2	0.28	0.63	0.20	0.37	0.08	0.08	0.58	29	0.40	1.90
35	14.2	0.30	0.75	0.33	0.53	0.15	0.15	0.65	31	0.45	1.60
36	24.2	0.31	0.69	0.18	0.71	0.05	0.07	0.48	34	0.28	3.90
37	24.2	0.25	0.50	0.18	0.50	0.07	0.08	0.45	34	0.38	2.80
38	29.2	0.30	0.50	0.21	0.47	0.05	0.07	0.33	37	0.24	2.40
39	29.2	0.28	0.50	0.26	0.42	0.05	0.07	0.47	37	0.20	2.40
40	34.2	0.30	0.46	0.15	0.35	0.04	0.04	0.26	39	0.27	2.30
41	34.2	0.38	0.59	0.21	0.58	0.05	0.06	0.39	39	0.24	1.80
42	34.2	0.30	0.43	0.27	0.46	0.03	0.07	0.33	40	0.11	1.70
43	39.2	0.30	0.49	0.11	0.45	0.01	0.05	0.47	43	0.10	4.10
44	44.4	0.30	0.45	0.12	0.37	0.01	0.05	0.40	44	0.09	3.10

3. 3. 2. Fluctuation of built-up edge in a continuous cutting.

In cutting under identical condition, growth and fracture of the built-up edge alternates so that its size fluctuates continually. The test data show that a thicker built-up edge (greater u) is accompanied by a longer contact with the chip (greater L), as illustrated by three selected test results in Fig. 10.

TABLE 3. Response of the metal cutting model geometries to the change in cutting conditions.

Item	When built-up edge grows in a continuous out so that the thickness u is increased	When cutting speed v is increased	When tool rake angle α is increased
Thickness of built-up edge u is		decreased	decreased
Contact length L is	increased	increased	decreased
Chip thickness t_2 is	unaffected	unaffected	decreased
Inclination of start plane of primary flow Φ is	unaffected	unaffected	increased
Distance T between G and H is	increased	decreased	decreased
Over-cut depth ψ is	unaffected	decreased	decreased
Thickness of distorted layer over finished surface h is	increased	decreased	decreased

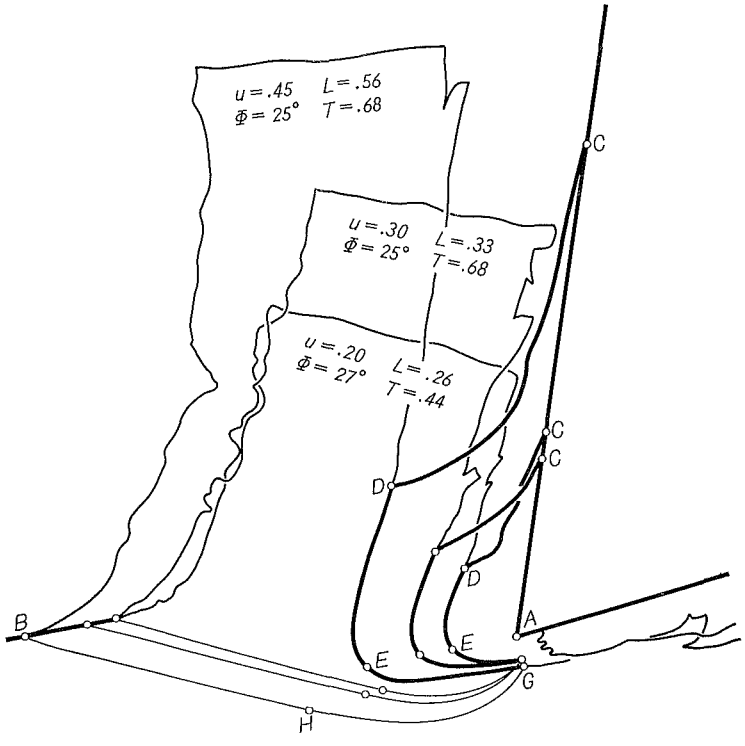

Fig. 10. Fluctuation of built-up edge in a continuous cutting. Depth of cut $t_1=0.3$ mm, Cutting speed $v=17$ mpm, 5% Co type high speed steel tool.

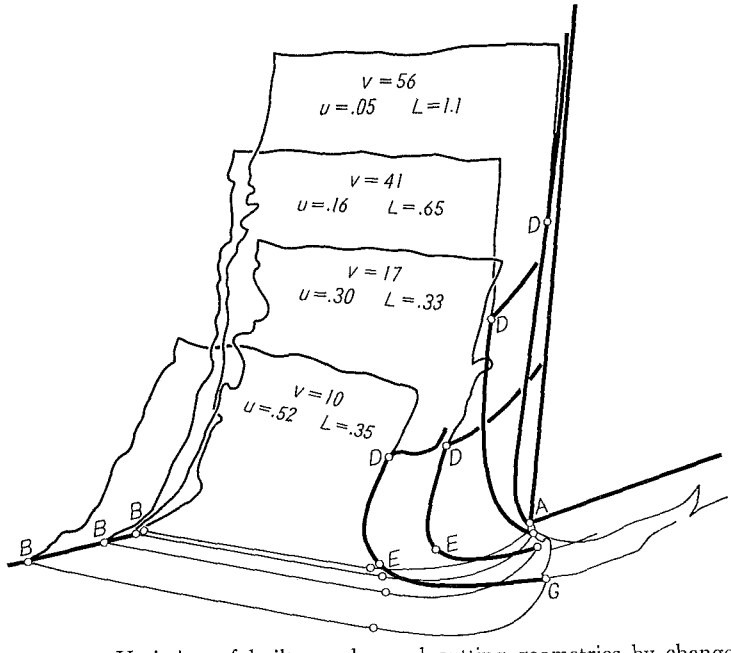

Fig. 11. Variation of built-up edge and cutting geometries by change in cutting speed v mpm. Depth of cut $t_1=0.3$ mm. u indicates thickness of built-up edge, L contact length both in mm. 5% Co type high speed steel tool.

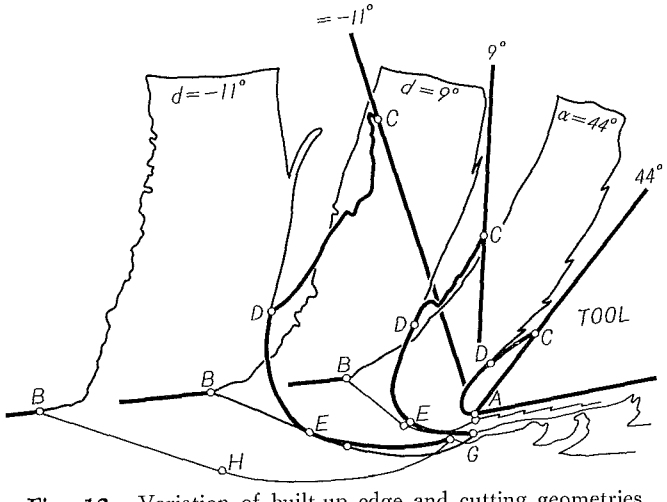

Fig. 12. Variation of built-up edge and cutting geometries by change in tool rake angle α.
Depth of cut $t_1=0.3$ mm, cutting speed $v=17$ mpm, 5% Co type high speed steel tool.

3. 3. 3. Effect of cutting speed on the built-up edge and cutting geometries.

Increased cutting speed brings about a thinner built-up edge (less u) as is commonly known, but a longer contact with the chip is present (greater L) as illustrated by four test results in Fig. 11. It is not clear whether the chip thickness t_2 is effected by those variations.

3. 3. 4. Effect of tool rake angle on the built-up edge and cutting geometries.

Cutting by a tool with a greater rake angle results in a smaller built-up edge (less u), a shorter contact (less L), and a thinner chip (less t_2) as illustrated in Fig. 12.

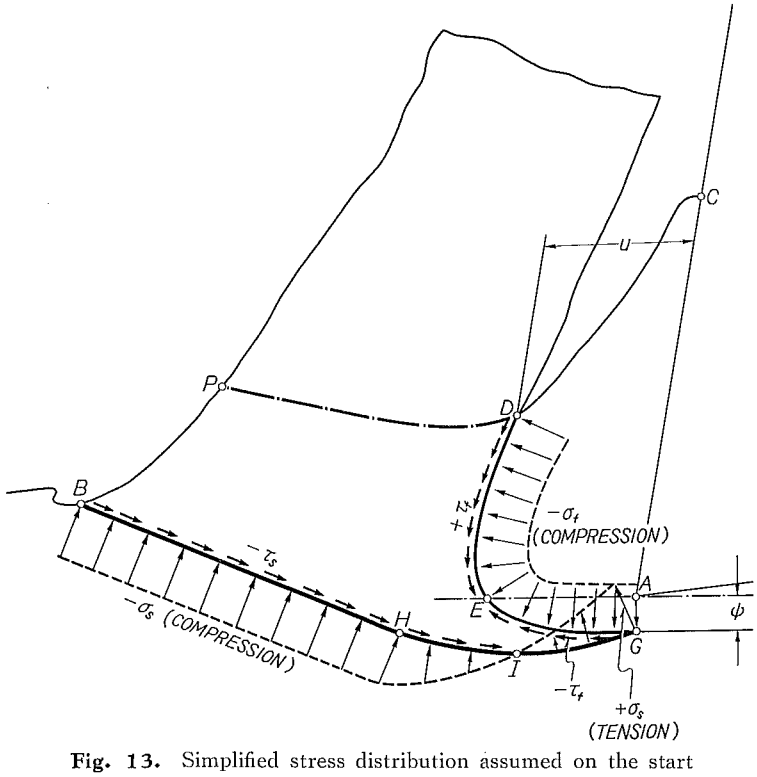

Fig. 13. Simplified stress distribution assumed on the start plane of primary flow BHIG and the built-up edge boundary DEG.

4. Analytical simulation of the metal cutting model with built-up edge.

4.1. Purpose of simulation.

In order to simulate the principle which ruled the variations of the built-up

edge and the metal cutting model geometries as observed in the preceding chapter, the equilibrium of cutting force was computed for the 44 test conditions, in such a may that the normal to shear stress ratios were obtained on the start boundary of primary flow and on the built-up edge boundary, based on the observed metal cutting geometries.

4. 2. Method of simulation.

a. (Assumptions on the start boundary of primary flow) As proposed in the metal cutting model, the work metal started a primary plastic flow when it crossed the boundary surface BHIG (Fig. 13). A simplified assumption was made in which the shear strain and therefore the maximum shear stress on the start boundary was acting in the direction along the boundary itself. As illustrated in Fig. 13, the magnitude of the maximum shear stress was denoted by $-\tau_s$ and it was uniformly distributed. The normal stress to the start boundary was assumed constant and was denoted by $-\sigma_s$ (compression) along the straight part of the start boundary BH, while it varied linearly along the curved part HIG in such a way that a tensile stress of $+\sigma_s$ was attained at the end point G.

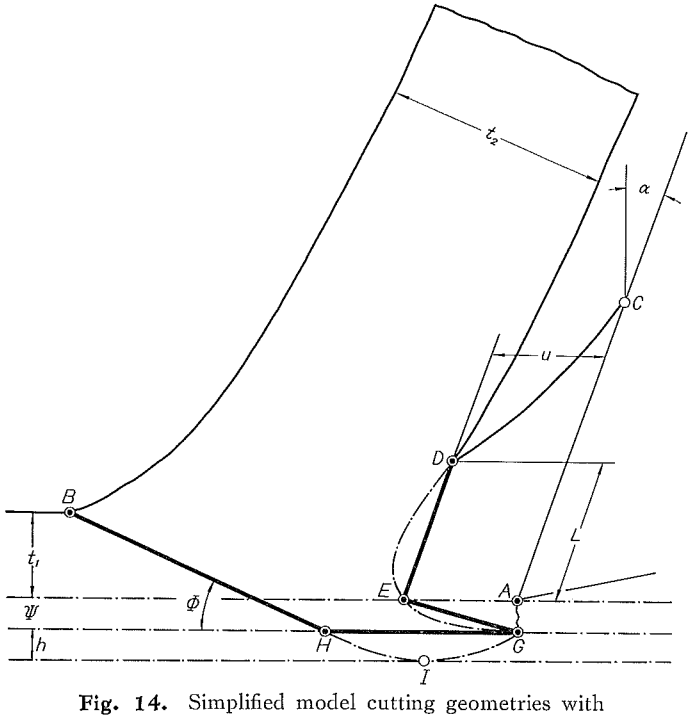

Fig. 14. Simplified model cutting geometries with the built-up edge.

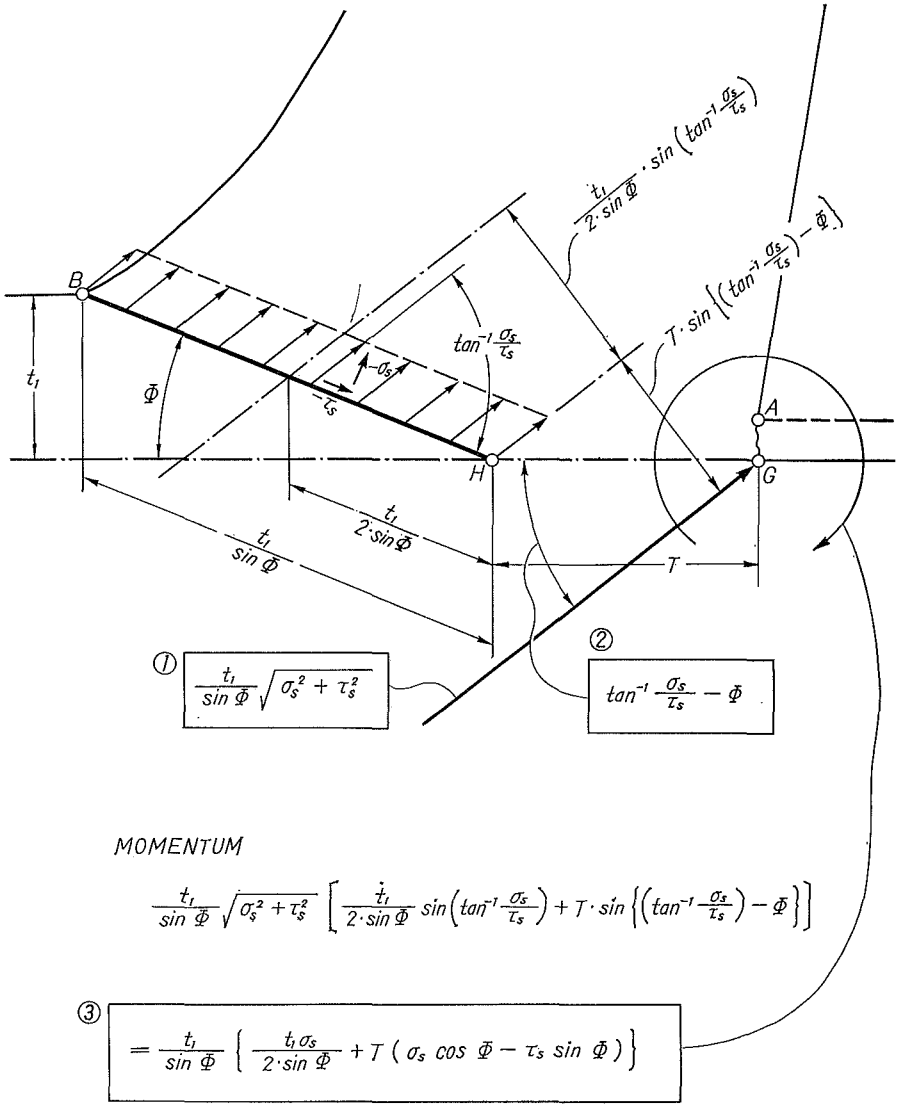

Fig. 15. Equilibrium equations on the plane B-H.

(1) magnitude of force
(2) direction of force
(3) momentum

b. (Assumptions on the built-up edge bondary) Along the built-up edge boundary, a uniform shear stress, which magnitude was denoted by τ_f, was assumed since the stationary built-up edge adjoined the deforming secondary flow region over this boundary. Opposite to the shear on the upper part of the built-up edge boundary DE, the lower part EG slides over the underlying metal, so that the sign of the shear stress was negative on the latter part. Normal stress to the built-up edge boundary was simply assumed to be uniform and was designated by $-\sigma_f$. Among the stress ratios: $s_1=\sigma_f/\tau_f$, $s_2=\sigma_s/\tau_f$, and $s_3=\tau_s/\tau_f$, defined from the above stress assumptions, an equation $(s_1+s_2)^2+s_3=1$ should hold according to the Mohr's stress circle at the point G.

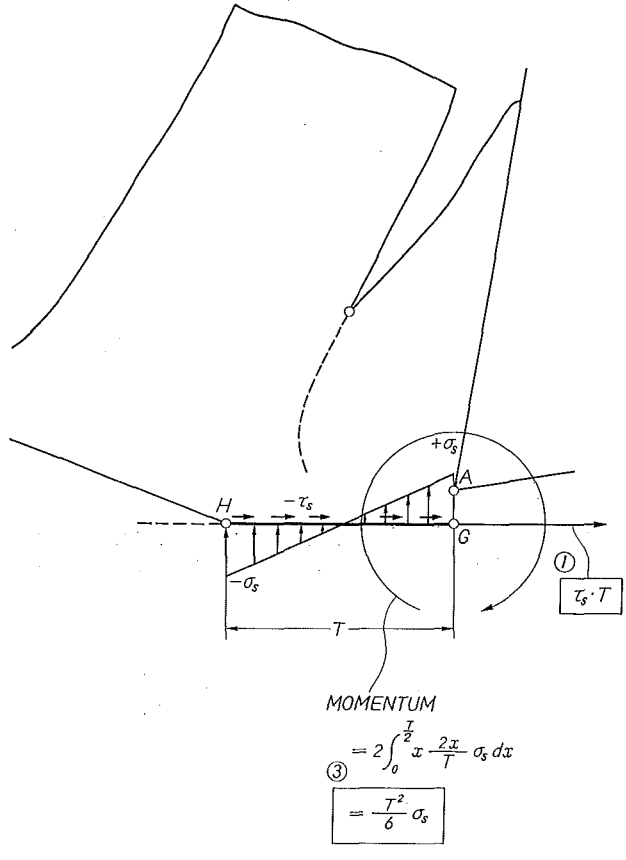

Fig. 16. Equilibrium equations on the plane H–G.

c. (Equilibrium equation of the force) With the curved portions of the two boundary surfaces further approximated by straight planes as shown in Fig. 14, (1) the magnitude of the resultant cutting force, (2) the direction of the resultant cutting force and (3) the resultant momentum of the cutting force were analytically derived on both of the two boundaries as illustrated in Fig. 15 to 20 and were equated to each other according to the equilibrium theory.

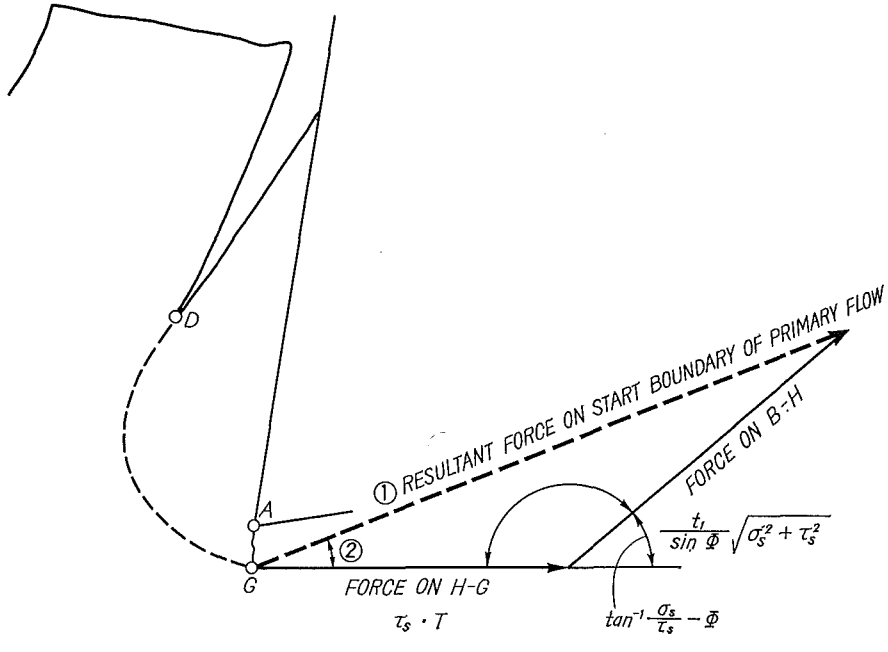

①

$$\sqrt{\tau_s^2 T^2+\frac{t_1^2}{\sin^2\Phi}(\sigma_s^2+\tau_s^2)+2\frac{\tau_s\cdot t_1\cdot T}{\sin\Phi}\sqrt{\sigma_s^2+\tau_s^2}\cdot\cos\left\{\left(\tan^{-1}\frac{\sigma_s}{\tau_s}\right)-\Phi\right\}}$$

②

$$\sin^{-1}\left\{\frac{t_1}{\sin\Phi}(\sigma_s\cdot\cos\Phi-\tau_s\sin\Phi)\Big/\sqrt{\tau_s^2 T^2+\frac{t_1^2}{\sin\Phi}(\sigma_s^2+\tau_s^2)+2\frac{\tau_s\cdot t_1\cdot T}{\sin\Phi}(\tau_s\cos\Phi+\sigma_s\sin\Phi)}\right\}$$

Fig. 17. Resultant equilibrium equations on the plane B-H and H-G.

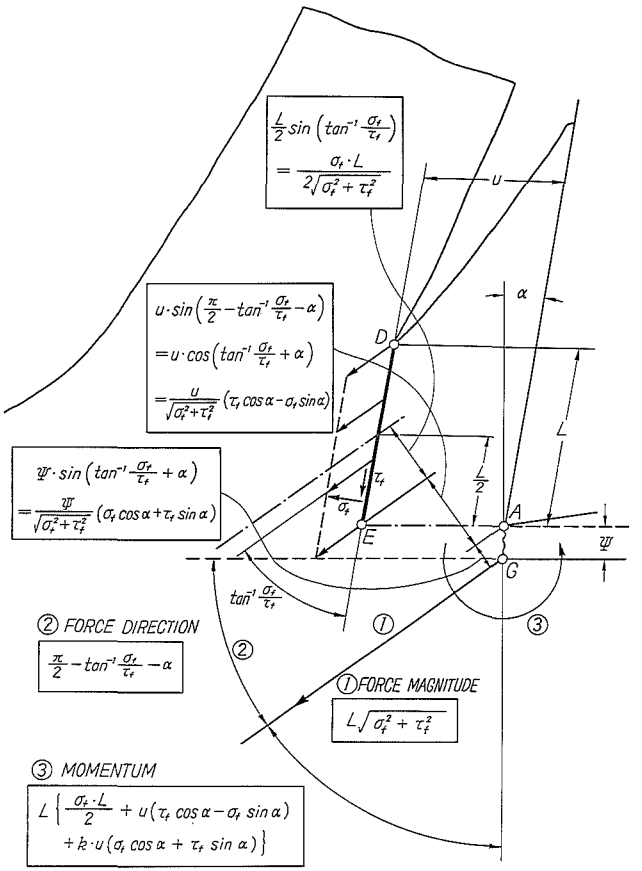

Fig. 18. Equilibrium equations on the plane D–E.

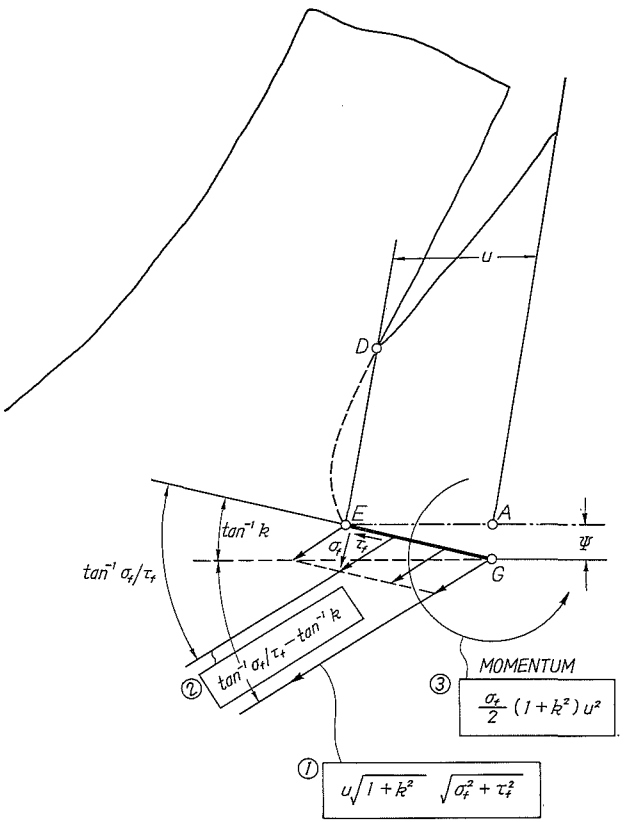

Fig. 19. Equilibrium equations on the plane E–G.

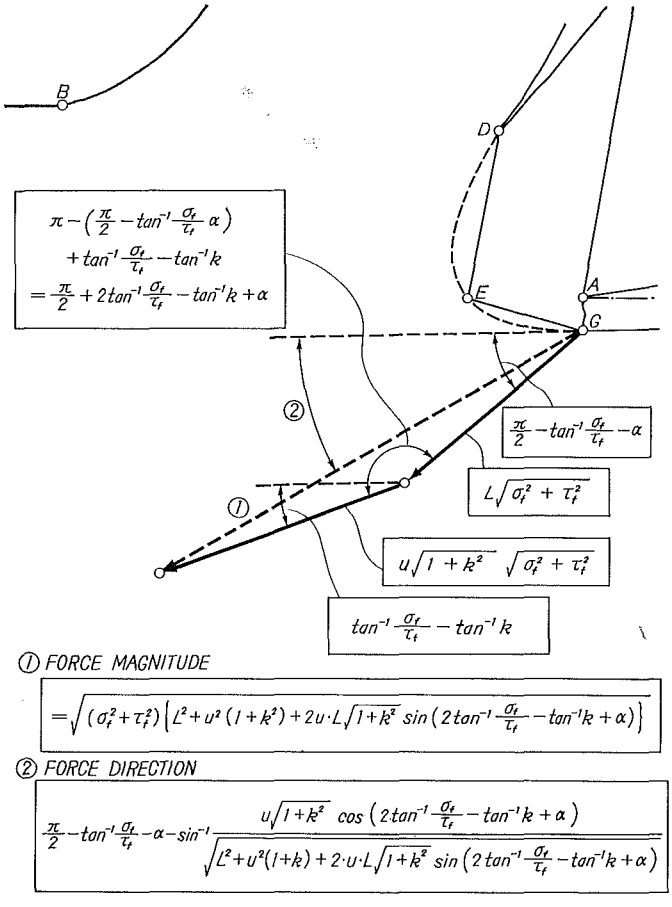

Fig. 20. Resultant equilibrium equations on the plane D-E and E-G.

d. (Computation of the force equilibrium) The derived equation contained in its variables, the cutting geometries ϕ, u, L, T, Φ, the cutting parameters α, t_1 and the stress ratios s_1, s_2, and s_3. The first seven variables were given their values from experimental data, and the unknown stress ratios were determined by a digital computer in such a way that the equilibrium equation was satisfied at the best. The computation flow diagram is shown in Fig. 21, and the computed values are presented in Table 4 and Table 5.

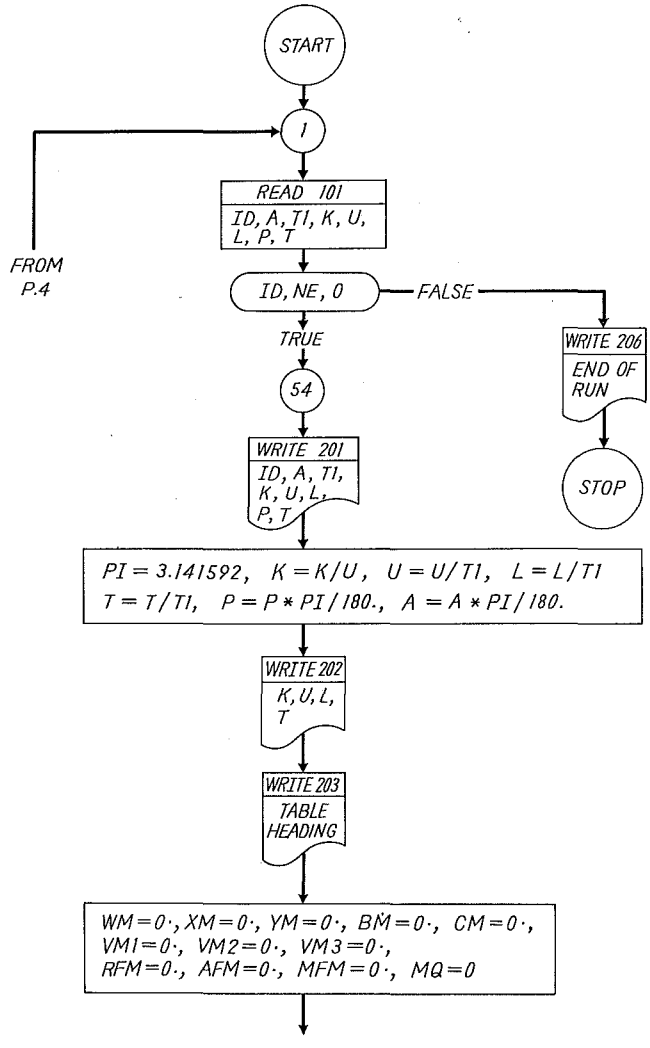

Fig. 21. Computer block diagram

(continued)

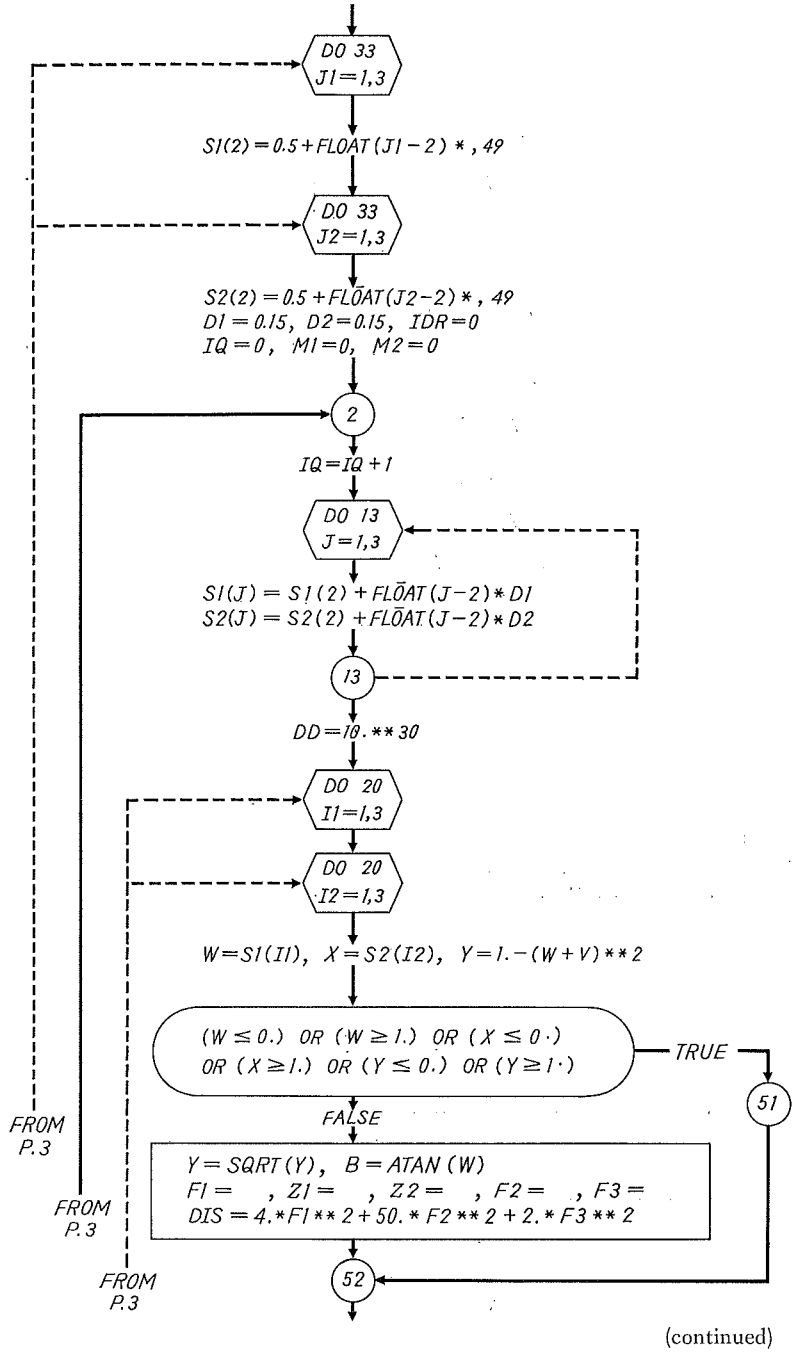
DO 33
J1=1,3
S1(2)=0.5+FLOAT(J1-2)*,49
DO 33
J2=1,3
S2(2)=0.5+FLOAT(J2-2)*,49
D1=0.15, D2=0.15, IDR=0
IQ=0, M1=0, M2=0
2
IQ=IQ+1
DO 13
J=1,3
S1(J)=S1(2)+FLOAT(J-2)*D1
S2(J)=S2(2)+FLOAT(J-2)*D2
13
DD=10.**30
DO 20
I1=1,3
DO 20
I2=1,3
W=S1(I1), X=S2(I2), Y=1.-(W+V)**2
(W≤0.) OR (W≥1.) OR (X≤0.)
OR (X≥1.) OR (Y≤0.) OR (Y≥1.)
TRUE
51
FALSE
Y=SQRT(Y), B=ATAN(W)
F1= , Z1= , Z2= , F2= , F3=
DIS=4.*F1**2+50.*F2**2+2.*F3**2
52
FROM P.3
FROM P.3
FROM P.3

(continued)

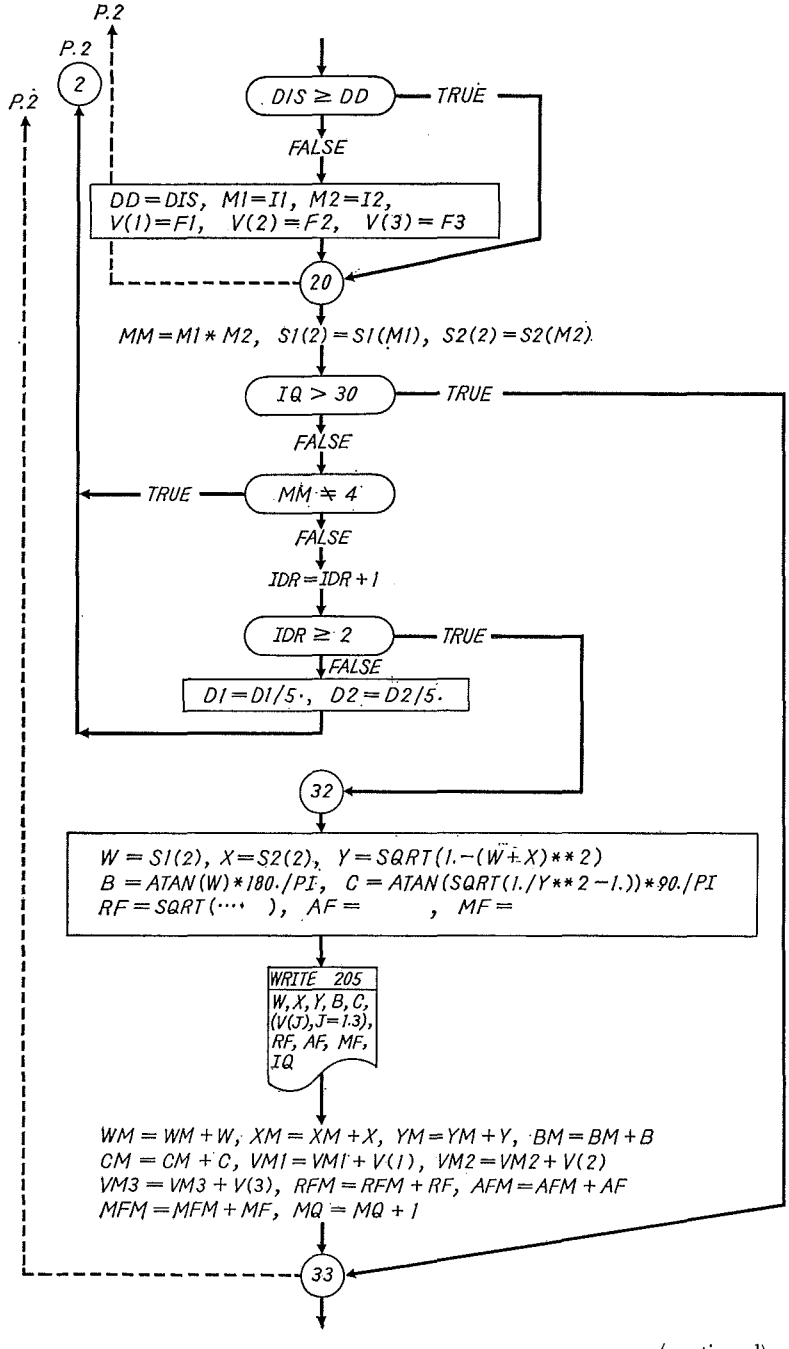
P.2
P.2
2
P.2
DIS ≥ DD
TRUE
FALSE
DD=DIS, M1=I1, M2=I2,
V(1)=F1, V(2)=F2, V(3)=F3
20
MM=M1*M2, S1(2)=S1(M1), S2(2)=S2(M2)
IQ > 30
TRUE
FALSE
TRUE
MM ≠ 4
FALSE
IDR=IDR+1
IDR ≥ 2
TRUE
FALSE
D1=D1/5., D2=D2/5.
32
W=S1(2), X=S2(2), Y=SQRT(1.-(W+X)**2)
B=ATAN(W)*180./PI, C=ATAN(SQRT(1./Y**2-1.))*90./PI
RF=SQRT(····), AF= , MF=
WRITE 205
W, X, Y, B, C,
(V(J), J=1.3),
RF, AF, MF,
IQ
WM=WM+W, XM=XM+X, YM=YM+Y, BM=BM+B
CM=CM+C, VM1=VM1+V(1), VM2=VM2+V(2)
VM3=VM3+V(3), RFM=RFM+RF, AFM=AFM+AF
MFM=MFM+MF, MQ=MQ+1
33

(continued)

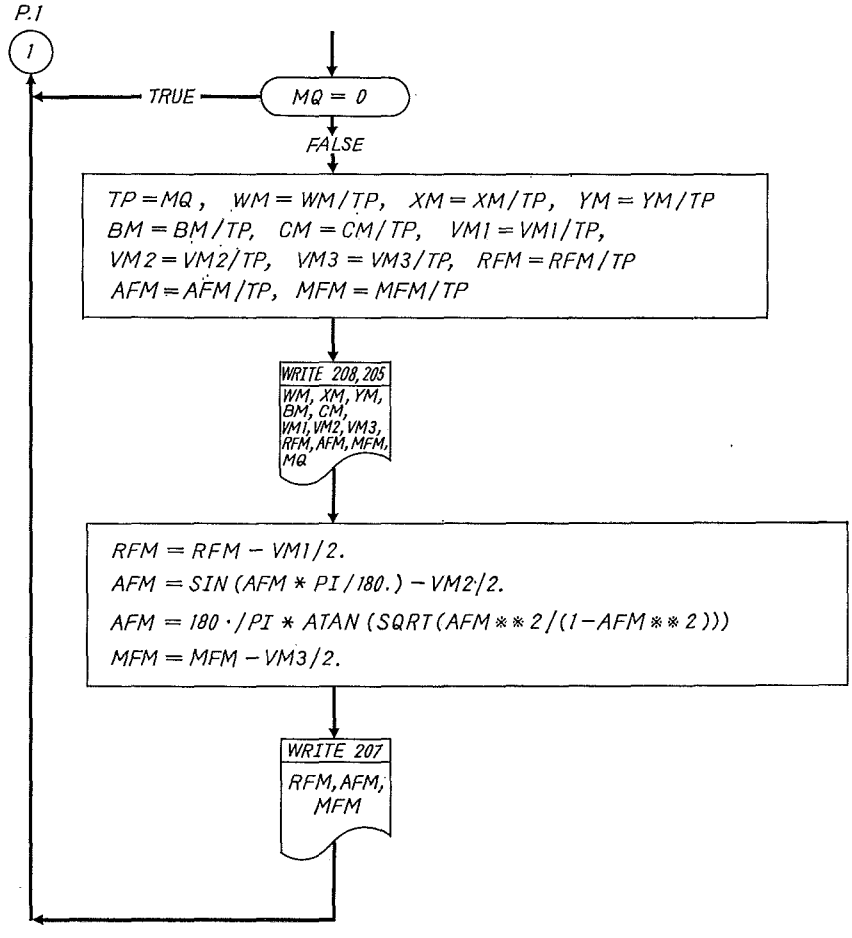
P.1
1
TRUE
MQ = 0
FALSE
TP=MQ, WM=WM/TP, XM=XM/TP, YM=YM/TP
BM=BM/TP, CM=CM/TP, VM1=VM1/TP,
VM2=VM2/TP, VM3=VM3/TP, RFM=RFM/TP
AFM=AFM/TP, MFM=MFM/TP
WRITE 208,205
WM, XM, YM,
BM, CM,
VM1, VM2, VM3,
RFM, AFM, MFM,
MQ
RFM = RFM - VM1/2.
AFM = SIN (AFM * PI/180.) - VM2/2.
AFM = 180./PI * ATAN (SQRT(AFM**2/(1-AFM**2)))
MFM = MFM - VM3/2.
WRITE 207
RFM, AFM,
MFM

TABLE 4. Computed values of cutting force, direction of force and momentum by change in cutting speed v.

Test No.	deg $B=\tan^{-1}\frac{\tau_f}{\sigma_f}$	deg $C=\Phi'$	$\frac{R}{t_1\tau_f}$	deg Direction of Resultant Cutting Force	$\frac{M}{t_1^2\tau_f}$
(1)	5.33	29.86	3.702	24.66	6.628
(4)	16.83	29.73	2.728	17.02	2.998
(2)	23.02	33.48	2.309	20.65	2.423
(3)	23.51	34.24	2.232	24.38	2.389
(16)	15.82	31.45	2.969	24.68	3.858
(10)	21.06	32.76	2.491	22.52	2.682
(7)	20.05	32.43	2.598	20.41	3.023
(5)	20.55	32.09	2.804	22.49	3.376
(6)	15.29	32.76	2.394	23.72	2.707
(11)	24.94	34.24	2.139	21.27	2.084
(13)	26.56	35.05	1.979	22.54	1.887
(8)	—	—	—	—	—
(9)	26.79	35.05	2.059	23.67	2.024
(12)	22.05	34.24	2.041	25.71	2.037
(14)	30.54	36.91	1.587	21.76	1.365
(15)	27.25	35.93	1.852	26.13	1.776
(17)	10.39	31.45	3.305	28.64	4.766
(18)	4.00	33.73	2.828	37.67	3.702
(20)	18.09	32.76	3.024	29.75	3.610
(19)	21.30	36.91	2.289	43.92	2.519
(21)	17.57	33.48	3.138	35.91	3.140
(22)	22.62	38.03	2.206	38.65	2.164
(23)	16.64	38.03	2.523	48.06	1.987

4.3. Result of simulation.

For various cutting speeds and tool rake angles, the simulation presented the stress ratio $s_1=\sigma_f/\tau_f$: the normal to shear stress ratio which most probably existed on the built-up edge boundary, and that on the start boundary of the primary flow. Also the magnitude of the resultant cutting force, its direction and the resultant momentum of the cutting force were predicted.

TABLE 5. Computed values of cutting force, direction of force and momentum by change in tool rake angle α.

Test No.	deg α	deg $B=\tan^{-1}\frac{\sigma_f}{\tau_f}$	deg $C=\Phi'$	$\frac{R}{t_1\tau_f}$	deg Direction of Resultant Cutting Force	$\frac{M}{t_1^2\tau_f}$
(24)	− 11.0	11.86	32.76	3.961	24.67	10.23
(25)	− 5.8	12.95	32.76	3.282	25.82	6.762
(26)	− 5.8	4.95	32.76	4.684	31.01	15.66
(27)	0	11.86	35.64	2.609	34.46	4.529
(28)	0	—	—	—	—	—
(29)	4.2	22.94	31.45	4.534	22.03	8.778
(30)	4.2	23.11	33.73	2.833	26.13	4.241
(31)	9.0	21.47	12.31	3.331	25.31	5.300
(32)	9.0	18.09	35.05	2.548	29.38	3.728
(33)	9.0	17.22	36.05	2.305	34.01	3.241
(34)	14.2	27.02	38.03	1.853	27.98	2.100
(35)	14.2	15.64	35.05	2.337	26.94	3.126
(36)	24.2	12.77	38.03	2.226	36.15	2.386
(37)	24.2	14.39	36.91	2.183	30.61	2.496
(38)	29.2	11.13	36.91	1.873	30.46	1.666
(39)	29.2	13.31	35.93	2.050	25.65	2.000
(40)	34.2	17.37	36.91	1.515	25.25	1.056
(41)	34.2	19.79	36.91	1.465	23.02	1.017
(42)	34.2	4.38	35.93	1.975	28.36	1.668
(43)	39.2	20.30	38.03	1.641	22.77	1.153
(44)	44.4	21.06	38.03	1.481	20.09	0.9249

The contact length between the built-up edge and the chip, in particular, was found to corelate well with the resultant force magnitude, as shown in Fig. 22, irrespective of the cutting speed and the tool rake angle. This prediction agrees with the well-known fact that the cutting force reduces with the built-up edge, so that this fact is possibly attributed to the reduced contact length, instead of the increased effective rake angle as was formerly conceived.

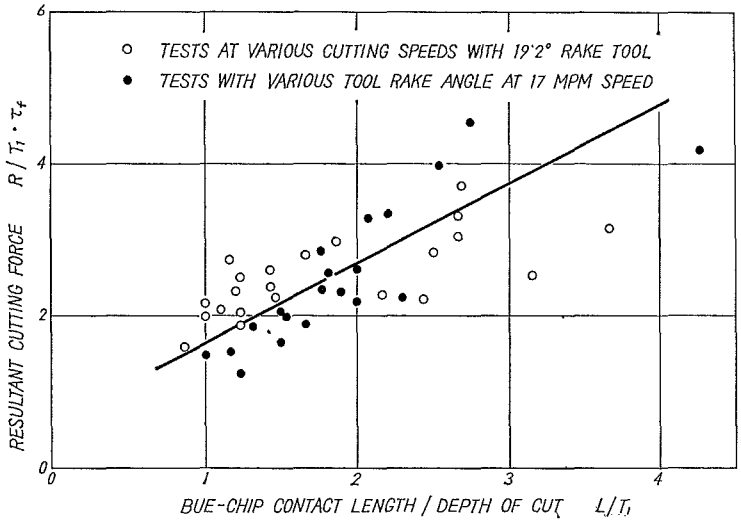

Fig. 22. Predicted corelation of built-up edge-chip contact length L to resultant cutting force R. (Result of computer simulation)

References

1) W. Rosenhain and A. C. Sturney: Flow and Rupture of Metals during Cutting, Proc. I.M.E. 1, 1925.
2) Diggs and Herbert: Proc. I.M.E. 1928.
3) H. Ernst and M. Martelotti: Die Bildung und Wirkung der "Aufbauschneide", Werkzeugmaschine, Heft 18, 1936.
4) V. D. Prianishnikoff: Am. Machinist, 180, 1936.
5) Rikichi Muranaka: Research paper of Toyama University.
6) M. E. Merchant: Tool Engineers Handbook, A.S.T.E., 1949.
7) Koichi Hoshi: On the Built-up Edge and Counter-plot for it, J.S.M.E., Abst., 1937.
8) Koichi Hoshi: On the Characteristics in the Cutting Action of Steel and Cast Iron, J.S.M.E., 1938.

Nomenclatures

(Cutting conditions)

α : rake angle of orthogonal cutting tool, deg
v : cutting speed, mpm (meters per minute)
t_1 : depth of cut in orthogonal cutting, mm
Hv: micro-Vickers hardness number

(Metal cutting geometries, refering to Fig. 6)

u : thickness of built-up edge measured in the cutting direction at point D, mm

L : contact length between built-up edge and chip measured parallel to tool rake face, mm

Φ : angle of the start boundary of primary plastic flow to the cutting direction, deg

ψ : over-cut depth, mm

h : depth of deformed layer, mm

T : distance between point H and G, mm

t_2 : chip thickness, mm

(Stress assumptions, refering to Fig. 13)

τ_s : shear stress on the start boundary of primary flow

σ_s : normal stress to the start boundary of primary flow

τ_f : shear stress on the built-up edge boundary

σ_f : normal stress to the built-up edge boundary

$s_1=\sigma_f/\tau_f$

$s_2=\sigma_s/\tau_f$

$s_3=\tau_s/\tau_f$